Published in final edited form as:
J Mol Cell Cardiol. 2013 March ; 56: 81–90. doi:10.1016/j.yjmcc.2012.12.004.

CypD$^{-/-}$ Hearts HaveAltered Levels of Proteins Involved in Krebs Cycle, Branch Chain Amino Acid Degradation and Pyruvate Metabolism

Sara Menazza[1,*], **Renee Wong**[1,*], **Tiffany Nguyen**[1], **Guanghui Wang**[2], **Marjan Gucek**[2], and **Elizabeth Murphy**[1]

[1]System Biology Center, National Heart, Lung, and Blood Institute, National Institutes of Health, Bethesda, MD

[2]Proteomics Core Facility, National Heart, Lung, and Blood Institute, National Institutes of Health, Bethesda, MD

Abstract

Cyclophilin D (CypD) is a mitochondrial chaperone that has been shown to regulate the mitochondrial permeability transition pore (MPTP). *MPTP opening is a major determinant of mitochondrial dysfunction and cardiomyocyte death during ischemia/reperfusion (I/R) injury.* Mice lacking CypD have been *widely* used to study regulation of the MPTP*, and it has been shown recently that genetic depletion of* CypD *correlates with elevated levels of mitochondrial* Ca^{2+}*. The present study aimed to characterize the metabolic changes in CypD*$^{-/-}$ *hearts. Initially, we* used a *proteomics* approach to examine protein changes in CypD$^{-/-}$ mice. Using pathway analysis we found that CypD$^{-/-}$ hearts have alteration in branched chain amino acid metabolism, pyruvate metabolism and the Krebs cycle. We tested whether these metabolic changes were due to inhibition of electron transfer from these metabolic pathways into the electron transport chain. As we found decreased levels of succinate dehydrogenase and electron transfer flavoprotein *in the proteomics analysis,* we examined whether *activities* of these enzymes might be altered*. However,* we found no *alterations in* their *activities. The proteomics study also showed a* 23% decrease in carnitine -palmitoyltransferase 1 (CPT1*), which prompted us to perform a metabolomics analysis. Consistent* with *the* decrease in *CPT1, we found a significant decrease in C4/Ci4, C5-OH/C3-DC, C12:1, C14:1, C16:1, and C20:3* acyl *carnitines in hearts from CypD*$^{-/-}$ *mice.* In summary, CypD$^{-/-}$ hearts exhibit changes in *many* metabolic pathways and caution should be used when interpreting results from these mice as due solely to inhibition of the MPTP.

Introduction

Cyclophilin D (CypD) is a mitochondrial peptidyl-prolyl cis-trans isomerase that has been shown to regulate the mitochondrial permeability transition pore (MPTP) [1–3]. Mice lacking CypD have been used to study the MPTP [4–6]*, and given* the widespread use of these mice [6–11] it is important to characterize proteomic changes that occur in these mice.

Correspondence: Elizabeth Murphy, National Heart, Lung, and Blood Institute, National Institutes of Health, Building 10, Room 8N202, 10 Center Drive, Bethesda, MD 20892, Phone: 301-496-5828, Fax: 301-402-0190, murphy1@mail.nih.gov.
*contributed equally

Disclosures: None.

There has been considerable interest in CypD because it is a regulator of the MPTP, a large conductance channel that can form in the inner mitochondrial membrane allowing passage of solutes and proteins less than 1.5 kDa [1, 12, 13]. The MPTP is activated by high matrix Ca^{2+} and reactive oxygen species (ROS) that occur in the setting of ischemia and reperfusion *(I/R)* [12], and the MPTP has been shown to be an important mediator of necrotic cell death [4, 14–16]. Inhibitors of MPTP, such as cyclosporine A (CsA), have been shown to reduce *I/R* injury in animal models as well as in humans [14, 15, 17, 18]. CsA inhibition of the MPTP occurs by binding to CypD [3]. Genetic deletion of CypD has also been shown to reduce *I/R* injury, presumably by inhibiting the prolonged opening of the MPTP [4, 5].

Previous studies have shown that $CypD^{-/-}$ hearts have increased matrix Ca^{2+}, increased activation of Ca^{2+}-activated mitochondrial dehydrogenases, and decreased fatty acid metabolism [6]. However, the mechanisms responsible for alterations in metabolism are poorly understood. We therefore undertook a proteomic analysis of mitochondria from $CypD^{-/-}$ hearts. Loss of CypD resulted in changes in a number of mitochondrial proteins and metabolic pathways, such as *the* Krebs cycle, branched chain amino acid *degradation* and propionoate metabolism. These changes suggest that caution should be used when interpreting changes in $CypD^{-/-}$ hearts solely to changes in the MPTP.

Materials and Methods

Animals

All animals were treated and cared for in accordance with the *Guide for the Care and Use of Laboratory Animals* [National Institutes of Health (NIH), Revised *2011*], and protocols were approved by the Institutional Animal Care and Use Committee. Male and female $CypD^{-/-}$ *and CypD-WT* mice were kindly provided by Dr. Jeffrey Molkentin (University of Cincinnati, Children's Hospital Medical Center). *The mice were between 12 and 16 weeks old at the time of experimentation and all the experiments were performed in the morning. The sex of the animals used is stated in each figure legend.*

Isolated Mouse Heart Preparation

$CypD^{-/-}$ mice were anesthetized with an intraperitoneal injection of 0.10 cc pentobarbital sodium diluted 1:5 in perfusate. The abdominal cavity was exposed with a transverse incision and 0.05 cc heparin was administered to the inferior vena cava. The heart was quickly isolated and placed in ice-cold Krebs-Heinseleit (KH) buffer (25 mM $NaHCO_3$, 120 mM NaCl, 11 mM glucose, 4.7 mM KCl, 1.2 mM KH_2PO_4, 1.2 mM $MgSO_4$, and 1.75 mM $CaCl_2$) to arrest the heart. The heart was perfused via the aorta. A water-filled latex balloon was inserted into the left ventricle to measure hemodynamic parameters using a PowerLab 2/25 and Chart v5.5 software (AD Instruments). All hearts were perfused with KH buffer gassed with 95% O_2 and 5% CO_2 and maintained at 37°C.

Mitochondria Isolation

Mitochondria were isolated by differential centrifugation according to standard procedures [19]. After rinsing out the blood, hearts were minced in 225 mM mannitol, 75 mM sucrose, 5 mM MOPS, 0.5 mM EGTA, and 2 mM taurine (pH 7.25) (Buffer B), and homogenized by Polytron. To digest contractile proteins *and obtain both interfibrillar and subsarcolemmal mitochondria*, trypsin (0.001 g/0.1 g wet tissue) in Buffer B was added to the homogenate for 5 min on ice. Digestion was stopped by addition of 0.2% bovine serum albumin (BSA). The homogenate was centrifuged at 500 *g* and the resulting supernatant was spun at 11,000 *g* to pellet the mitochondria. The final mitochondrial pellet was resuspended in Buffer B*. For functional studies, 0.2% BSA was added to the mitochondrial suspension.*

2D Gel Electrophoresis

Hearts were perfused for 5 min in KH buffer, snap-frozen, and ground in lysis buffer (30 mM Tris-HCl, 7 M urea, 2 M thiourea, and 4% CHAPS (w/v)) with protease and phosphatase inhibitors (200 μg/mL phenylmethanesulfonyl fluoride (PMSF), 20 mM glycerophosphate, 1 mM sodium orthovanadate, 1 mM sodium fluoride, 10 μg/mL aprotinin, and 4 μg/mL leupeptin). Homogenates were centrifuged at 10,000 *g* for 2 min and protein concentration was determined on the resulting supernatant. Samples were cleaned by acetone precipitation before 2D electrophoresis. CyDye 2D fluorescence difference gel electrophoresis (DIGE) were performed as described previously [20]. Individual samples (50 μg) were labeled with Cy3 and Cy5 (GE Healthcare). A 50 μg internal standard consisting of equal protein amounts of all samples was labeled with Cy2. The labeled samples and internal standard were combined with 175 μg of each sample (unlabeled) to bring the total protein for each gel to 500 μg. First dimension isoelectric focusing was carried out on 24 cm Immobiline DryStrip gels pH 3–10 non-linear (GE Healthcare) in an Ettan IPG Phor electrophoresis unit (GE Healthcare) rehydrating at 30 V for 10–12 h followed by focusing for ~66,667 Vh. The strips were loaded into pre-cast 10–15% Optigel polyacrylamide gels (NextGen Sciences), and the proteins were separated on an Ettan DALT-12 electrophoresis unit (GE Healthcare) at constant voltage (~2350 Vh). All gels were scanned on a Typhoon 9400 variable imager (GE Healthcare) at a resolution of 100 μM. Image analysis was performed using the cross-stain analysis function with Progenesis Discovery software (NonLinear Dynamics).

Protein Identification

For all protein identifications from 2D gels, protein spots were picked using the Ettan Spot Handling Workstation (GE Healthcare). Protein identification was carried out using a MALDI-TOF/TOF instrument (4700 Proteomics Analyzer, Applied Biosystems,) with reflector positive ion mode. For MS analysis, 800–4000 *m*/*z* mass range was used with 1500 shots per spectrum. The Mascot search engine was used (version 2.2, Matrix Science) for peptide and protein identifications. The data searches were performed with the following search parameters: enzyme specificity was set to trypsin, one missed cleavage allowed, fixed modifications for cysteine carbamidomethylation and variable modifications set for methionine oxidation and a mass tolerance of 100 ppm and 0.5 Da was used for precursor ions and fragment ions, respectively. Swiss-Prot protein knowledgebase database (Sprot, release 57.4, 16-Jun-2009; 497,293 sequences) was searched against and MS peak filtering was set for all trypsin autolysis peaks. The species selected was *Mus musculus* (mouse) and the number of sequence entries searched in the *Mus musculus* database is 16,183 out of 497,293 total sequence entries. The identification of two peptides or more had to meet the following criteria: expectation value less than 0.5 and molecular weight had to match the position where the spot was picked on the 2D gel.

iTRAQ Labeling of CypD$^{-/-}$ Heart Mitochondria

Mitochondria isolated from two male and two female CypD$^{-/-}$ and WT hearts were used for iTRAQ studies. Prior to all labeling, mitochondrial samples were separated on NuPAGE 4–12% Bis-Tris gels (Invitrogen) and stained with Coomassie Blue to ensure similar protein content and complexity in all groups. Peptide labeling with isotope tags for relative and absolute quantification (iTRAQ) was performed as described previously [21]. In brief, individual mitochondrial samples were lysed in buffer containing 8 M urea, 2 M thiourea, 4% CHAPS (w/v), 75 mM NaCl, 50 mM Tris-HCl, 1 mM PMSF, 2 mM glycerophosphate, 1 mM sodium orthovanadate, 2 mM sodium fluoride, and 10 mM sodium pyrophosphate (pH 8.0) and sonicated on ice. Lysates were spun at 14,000 *g* at 4°C for 30 min and a Bradford assay was performed on the supernatant to obtain an optimal protein concentration of 5–8 mg/mL. The heart mitochondrial lysates (100 μg of each sample) were reduced with

5 mM dithiothreitol at 37°C for 1 h and alkylated with 80 mM iodoacetamide at 37°C for 1 h. Trypsin digestion (protein enzyme ratio of 25:1) was performed overnight at 37°C and desalted on Oasis HLB 1 cm^3 cartridges (Waters, Milford, MA) per manufacturer's instructions. Eluents were dried completely and reconstituted in 30 μL of iTRAQ dissolution buffer. One vial each of iTRAQ reagents 113, 115, 117, and 119 was used to label WT samples, while one vial each of iTRAQ reagents 114, 116, 118, and 121 was used to label $CypD^{-/-}$ samples at room temperature for 1 h 30 min. After labeling, the samples were combined and diluted to a total of 25 mL with 0.1% trifluoroacetic acid (TFA) before desalting on Oasis HLB 6 cm^3 cartridges (Waters) and dried completely.

Strong Cation Exchange Chromatography (SCX) of iTRAQ-Labeled Peptides

The dried peptides were reconstituted in 200 μL of SCX solvent A (5 mM KH_2PO_4, 25% acetonitrile (ACN), pH 2.67) and injected onto a PolySULFOETHYL A SCX column (4.6 mm i.d. × 20 cm length, 5 μM particle size, 300 Å pore size). Chromatography was performed on an Agilent HP1100 system at 1 mL/min flow rate using the following gradient: 0% solvent B (5 mM KH_2PO_4, 25% CAN, 500 mM KCl, pH 2.67) for 2 min; 0–70% solvent B for 35 min; 70–100% solvent B for 1 min; and 100% solvent B held for 4 min. UV absorbance as monitored at 214 nm and fractions collected at 1.5-mL intervals, which were subsequently dried completely. Fractions were desalted on Oasis HLB 1 cm^3 cartridges (Waters) prior to mass spectrometry (MS) identification.

LC-MS/MS Analysis

All dried fractions were analyzed on a LTQ-Orbitrap Velos (Thermo-Fisher Scientific) interfaced with an Eksigent nano-LC Ultra system (Eksigent Technologies) using high-energy collision dissociation (HCD). Briefly, samples were loaded onto an Agilent Zorbax 300SB-C_{18} trap column (0.3 mm i.d. ×5 mm length, 5 μm particle size) at a flow rate of 5 μL/min for 10 min. Reversed-phase C_{18} chromatographic separation of peptides was carried out on a prepacked BetaBasic C_{18} PicoFrit column (75 μm i.d. × 10 cm length, New Objective) at 300 nL/min using the following gradient: 2–5% B for 5 min; 5–40% B for 40 min; 40–50% B for 10 min; and 50–95% B for 5 min (solvent A, 0.1% formic acid in 98% water, 2% ACN; solvent B, 0.1% formic acid in 100% ACN). LTQ-Orbitrap Velos settings were as follows: spray voltage 1.2 kV, 1 microscan for MS1 scans at 30,000 resolution (fwhm at m/z 400), 2 microscans for MS2 at 7500 resolution (fwhm at m/z 400); full MS mass range, m/z 300–2000; MS/MS mass range, m/z 100–2000. The LTQ-Orbitrap Velos was operated in a data-dependent mode, that is, one MS1 FTMS scan for precursor ions followed by six data-dependent HCD-MS2 scans for precursor ions above a threshold ion count of 5000 with collision energy of 45%.

Database Search, iTRAQ Quantification, and Pathway Analysis

We used Proteome Discoverer 1.2 (Thermo Fisher Scientific) to search and quantify the iTRAQ data obtained on Orbitrap Velos. The processed spectra were searched on our six processor Mascot cluster at NIH (http://biospec.nih.gov, version 2.3) using the following criteria: database, Swiss-Prot; taxonomy, *Mus musculus* (mouse); enzyme, trypsin; miscleavages, 2; fixed modifications, carbamidomethylation (+57 Da), N-terminal iTRAQ8plex (+304 Da), lysyl iTRAQ8plex (+304 Da); variable modifications, methionine oxidation (+16 Da); MS peptide tolerance as 50 ppm; MS/MS tolerance as 0.05 Da. The false discovery rate (FDR) was set to 1%. For iTRAQ quantification, the ratios of iTRAQ reporter ion intensities in MS/MS spectra (m/z 113.11–121.11) from raw data sets were used to calculate fold changes in protein expression between WT and $CypD^{-/-}$ mice. Pathway analysis on the identified iTRAQ protein level changes was performed with Ingenuity Pathway Analysis Software (Ingenuity Systems, Redwood City, CA).

Electron Transfer Flavoprotein-Ubiquinone Dehydrogenase (ETFDH) Activity Assay

Mitochondria were prepared as indicated above and resuspended in 40 μl of 20 mM phosphate buffer saline, pH 7.5. Three *mitochondrial* heart preparations were combined together for each single experiment. *Mitochondria (3mg in* 120 μl of *buffer)* were sonicated two times for 20 sec and centrifuged at *100,000 g* for 1 h at 4°C. The resulting supernatant (50 μg*) was* mixed with 2 mM *N*-Ethylmaleimide (NEM), 0.288 mM octanoyl-coA, and 2.5 μM Medium-chain acyl-CoA dehydrogenase (MCAD, Fitzgerald Industries International Inc.). The ETFDH enzymatic activity was measured by monitoring the reduction of 120 μM 2, 6-dichloroindophenolate (600 nm) at 30°C as described [22]. Mitochondria *that were* denatured by incubation for 10 min at 60°C were used as control.

Succinate *Dehydrogenase* (SDH) Enzymatic Activity Assay

Mitochondria were prepared as indicated above and resuspended in a buffer containing 5 mM $MgCl_2$ and 25 mM potassium phosphate, pH 7.2. The mitochondria were freeze-thawed three times and sonicated for 1 min. Mitochondria (50μg) were resuspended in an assay buffer containing 5 mM $MgCl_2$, 25 mM potassium phosphate, 20 mM sodium succinate, 2 mM potassium cyanide, 2 μg/*mL* antimycin A, and 2 μg /*mL* rotenone (pH 7.2) at *30°C* for 10 min prior to the addition of 50 μM 2, 6-dichloroindophenolate and 56 μM ubiquinone (Coenzyme Q1) to fully activate the *SDH enzyme* [23]. SDH activity was measured by monitoring the absorbance of the reduction of 2, 6-dichloroindophenolate at 600 nm. Mitochondria *that were incubated* with 20mM sodium malonate *were* used as control.

Malate-Aspartate Shuttle (MAS) Activity

Heart mitochondria were prepared as above and resuspended in 100 μL of Buffer B. The MAS assay was adapted from Contreras and Satrustegui [24]. *Briefly,* 100 μg of mitochondria were mixed with 10 mM Tris (pH 7.4), 300 mM mannitol, 10 mM K_2HPO_4, 5 mM $MgCl_2$ and 10 μM KCl *prior to adding 4 units/mL aspartate aminotransferase, 6 units/mL malate dehydrogenase, 140 μM NADH, 5 mM aspartate, and 0.5 mM ADP.* Experiments were performed in a final volume of 200 μl using a black 96-well plate. Once a baseline *was* achieved, *MAS* shuttle activity was initiated by adding 5 mM glutamate and 5 mM malate and the decrease in NADH fluorescence was monitored at 340 nm (Fluostar Omega, BMG Labtech). All assays were performed at 37 °C. The rate of change of florescence was expressed as nanomoles of NADH oxidized per minute.

Metabolomics Analysis

After anesthesia hearts were collected, rinsed in saline buffer and the atria were removed. The samples were immediately frozen in liquid nitrogen, stored at −80°C and sent for the metabolomic analysis (Sanford Burnham Metabolomics core facility). Acyl carnitine was measured as described previously [25].

Oxygen Consumption

Mitochondrial O_2 consumption was measured using a YSI model 5300A Biological Oxygen Monitor (YSI Life Sciences,) with a Clark oxygen electrode and recorded with Chart5.0.1 software on a PowerLab 2/25 (AD Instruments). Mitochondria (300 μg) were loaded into a closed water-jacket reaction chamber (Harvard Apparatus #BS4 56-4930 flow chamber) maintained at 25°C. All experiments were performed in oxygen-saturated buffer containing 120 mM KCl, 1 mM EGTA, 5 mM MOPS, 5 mM KH_2PO_4, and 0.2% BSA (pH 7.25). The mitochondria were allowed to equilibrate in the chamber prior to adding 10 mM glutamate/2 mM malate or 5 mM succinate/ 2 μM rotenone (State 2). After 2 min, ADP (0.5 mM) was then added to initiate State 3 until depleted to reach State 4.

H_2O_2 Production

Hydrogen peroxide (H_2O_2) production from isolated heart mitochondria, which were energized with 10 mM glutamate/2 mM malate or 10mM succinate as substrates was monitored fluorimetrically by measurement of Amplex Red oxidation to fluorescent resorufin (Invitrogen).

Data Analysis

All data are presented as means ± SE. Statistics were performed using a Student t-test or a one-way ANOVA analysis followed by a Fishers LSD post-hoc test. A value of $p \leq 0.05$ was considered significant.

Results

Cardiac Proteome Differences in CypD$^{-/-}$ versus WT

To gain a better understanding of the targets of CypD and its physiological role, we investigated differences in the mitochondrial proteome of CypD hearts. We first used *a* two-dimensional difference in-gel electrophoresis (2D DIGE) proteomic *method* to examine changes in protein levels in total heart homogenates from *male and female* WT and CypD$^{-/-}$ mice. *We found similar differences between CypD−/− and WT in both sexes.* Figure 1 *is a representative 2D DIGE image comparing WT and CypD$^{-/-}$ female mice. We found 23 significant protein differences, between WT and CypD$^{-/-}$ mice present in both male and female mice* (Table 1). Of the 23 significant changes identified, there were only 8 protein changes that were greater than 20% in the CypD$^{-/-}$ mice relative to WT. The most striking effect in the CypD$^{-/-}$ mice was a ~3-fold increase in peroxiredoxin-6, a thiol-specific antioxidant protein that can scavenge H_2O_2.

iTRAQ Differences in Mitochondrial Proteome

As shown in Figure 1 and Table 1, there were only a modest number of protein differences greater than 20% in the CypD$^{-/-}$ hearts identified in the 2D DIGE. We therefore took a different approach and focused on mitochondrial proteins using a direct mass spectrometry method that allowed us to increase the protein amount (there is a limit to how much protein can be loaded on the gel) to identify additional protein alterations. We utilized isobaric tags for relative and absolute quantitation (iTRAQ) along with mass spectrometry to assess changes in mitochondrial proteins in CypD$^{-/-}$ mice. Mitochondrial fractions were isolated from WT and CypD$^{-/-}$ mice. Prior to iTRAQ labeling, the fractions were separated and stained with Coomassie Blue to ensure that similar protein bands were found in all samples (Figure 2). We found 30 proteins significantly decreased; 10 of these showed a 20% or greater decrease (Table 2). We performed a pathway analysis to identify the key signaling pathways affected by these protein decreases and found that these proteins were involved in mitochondrial dysfunction, branched chain amino acid (BCAA) degradation, butanoate metabolism, pyruvate metabolism, tricarboxylic acid (TCA) cycle, and oxidative phosphorylation (Figure 3A).

In addition to the protein decreases, we found 20 proteins increased in the CypD$^{-/-}$ mice; 8 of which showed a 20% or greater increase (Table 3). These protein changes were involved in pathways including mitochondrial dysfunction, ubiquinone biosynthesis, propanoate metabolism, BCAA degradation, and oxidative phosphorylation (Figure 3B). We identified only 2 common proteins in both iTRAQ and the 2D DIGE results (Table 1): acetyl-coenzyme A synthetase 2-like enzyme and the 60 kDa heat shock protein (HSP60). Acetyl-coenzyme A synthetase 2-like enzyme, which is involved in acetate oxidation, was decreased in the 2D DIGE (14%) and iTRAQ methods (16%) while HSP60 was elevated in

2D DIGE (11%) and iTRAQ (14%). Interestingly, HSP60 has been recently shown to form a complex with CypD and knockdown of HSP60 activates the MPTP in tumor cells [26].

Metabolic Changes in CypD$^{-/-}$ Hearts

We considered that the alterations in BCAA and other metabolic pathways might be due to an inhibition of the electron transfer flavoprotein (ETF) or the ETF-ubiquinone dehydrogenase (ETFDH) activity. Many BCAA metabolites donate electron to the electron transport chain via ETF/ETFDH, and an inhibition of ETFDH would lead to dysregulation of BCAA and fatty acid metabolism. We also observed a decrease in the level of both the alpha and beta subunit of ETF in the CypD$^{-/-}$ hearts (Table 2). We therefore measured ETFDH activity in mitochondria *isolated* from *male WT and* CypD$^{-/-}$ *mouse* hearts. As shown in Figure 4A, there was no difference in ETFDH activity between WT and CypD$^{-/-}$ heart mitochondria.

We found a decrease in two subunits (DHSB and C560) of succinate dehydrogenase (SDH) (Table 2). Furthermore, in previous studies, we found an increase in succinate in CypD$^{-/-}$ hearts. We considered that inhibition of succinate dehydrogenase (SDH) would lead to an increase in succinate. Therefore, we measured SDH, but found no difference between mitochondria *isolated from male WT and CypD$^{-/-}$mouse hearts* (Figure 4B). Next, we considered that the increase in succinate could be related to altered metabolism of α-ketoglutarate. α-ketoglutarate is converted to succinate via α-ketoglutarate dehydrogenase and succinylCoA synthase, and it is a key metabolite in the malate-aspartate shuttle (MAS). *The MAS facilitates the transfer of membrane*-impermeable *NAD(H) across* the inner mitochondrial membrane. *We found that* mitochondrial 2-oxoglutarate/malate carrier protein (M2OM*), a component* of the MAS*, was decreased* in the CypD$^{-/-}$ hearts. M2OM is *also a member* of *a protein* super family that includes adenine nucleotide transporter (ANT) and the phosphate carrier (PiC), which have been suggested to interact with CypD [27, 28]. *We considered that a* decrease in M2OM activity *may* lead *to* reduced α-ketoglutarate efflux from the mitochondria*, increased* α-ketoglutarate *levels in the matrix, and higher* succinate *levels*. We examined whether there were alterations in the MAS activity in *isolated* mitochondria *from male CypD$^{-/-}$ mouse hearts. We reconstituted* the complete shuttle by *incubating* isolated heart mitochondria with purified cytosolic enzymes of *the* MAS *(i.e.,* glutamate oxaloacetate transaminase and malate dehydrogenase). As shown in Figure 4C, we did not find a decrease in MAS activity, but rather we found increased activity of the shuttle in CypD$^{-/-}$ mitochondria. This result would be consistent with our previous observation suggesting a higher glycolytic flux in CypD$^{-/-}$ hearts, which would result in an increased production of cytosolic NADH that would enter the mitochondria via the shuttle.

Because many of the pathways that are altered in the CypD$^{-/-}$ mice involve generation of acyl CoA (*i.e.*, acetyl CoA, succinyl CoA etc), we evaluated the acyl carnitine profile in *these hearts*. As shown in Figure 5, we found *decreased* levels of several acyl carnitine metabolites (*i.e.*, C4/Ci4, C5-OH/C3-DC, C12:1, C14:1, C16:1, and C20:3). In light of our previous data showing the CypD$^{-/-}$ hearts have decreased fatty acid oxidation relative to glucose oxidation, this decrease in acylcarnitines would suggest a possible inhibition of carnitine O-palmitoyltransferase 1 (CPT1). Consistent with this, we found a 23% decrease in CPT1B (Table 2) in the CypD$^{-/-}$ hearts.

Oxygen Consumption in CypD$^{-/-}$ Mitochondria

Because of the observed decrease in levels of a few subunits of electron transport complexes (Table 2), we measured oxygen consumption of mitochondria isolated from WT and CypD$^{-/-}$ *male* hearts to evaluate whether there were differences in oxidative phosphorylation with succinate versus glutamate-malate (Figure 6). We found no significant

differences in respiration between WT and CypD$^{-/-}$ mitochondria using succinate/rotenone or glutamate/malate as substrates (Figure 6). We also measured whether loss of CypD led to differences in ROS production in the form of hydrogen peroxide (H_2O_2) using Amplex Red. As illustrated in Figure 7, there were no changes in H_2O_2 production between *mitochondria from male* WT and CypD$^{-/-}$ *mouse hearts* with either glutamate/malate (Figure 7A) or succinate/rotenone (Figure 7B) as substrates.

Discussion

The primary goal of this study was to identify proteomic differences between WT and CypD$^{-/-}$ mice to provide insight into the physiological function of CypD. CypD is a *mitochondrial* chaperone *that* has been previously reported to interact with a number of proteins (ANT, PiC, mitochondrial F_0-ATPase) [27–32]. Previous studies have shown that although CypD ablation reduces ischemia-reperfusion injury, it increases the susceptibility to heart failure and alters metabolism [6]. We measured protein changes in mice lacking CypD and identified changes in mitochondrial pathways involved in BCAA degradation, pyruvate metabolism, and the Krebs cycle. *For the proteomic studies we used males and females mice, and we found that the differences between CypD−/− and WT were present in both sexes. Therefore for the remainder of the studies we used only male mice.*

As indicated by pathway analysis, a large number of the *protein* changes in CypD$^{-/-}$ hearts occur in the BCAA degradation pathway. These include methylcrotonoyl-CoA carboxylase (both the A and B subunits), methylmalonyl-CoA mutase, enoyl CoA hydratase, lipoamide acyltransferase of branched chain keto-acid dehydrogenase, and 2-oxoisovalerate dehydrogenase subunit beta. Loss of CypD also resulted in changes in pathways involving pyruvate and fatty acid metabolism. These changes in metabolic pathways were not due to alterations in SDH or the ETFDH.

Measurement of MAS activity showed a significant increase in the capacity to transport reducing equivalents *of* cytosolic NAD(H) *to* the *mitochondrial* matrix in CypD$^{-/-}$ hearts. These data are consistent with our previous observation that carbohydrate oxidation is increased in the CypD$^{-/-}$ hearts. Glycolysis results in the production of cytosolic NADH, which is *transferred* into the mitochondria by MAS.

Although the proteomics data *showed* alterations in *enzymes* of many metabolic pathways, the *proteomics* data alone do not provide information about flux through *these* pathways. For example, an increase in an enzyme level could indicate an *increased* flux through that pathway or it could indicate that the enzyme is inhibited and *its* level is increased due to a feedback regulation. Because all the pathways involve alterations in acyl CoA, we measured the acyl *carnitine* profile as a surrogate for acyl CoA. As shown in Figure 5, we found a decrease in many acyl carnitines in the CypD$^{-/-}$ hearts. A decrease in long chain acyl carnitine levels would be consistent with *our observed* decrease in CPT1, an enzyme on the outer mitochondrial membrane that is responsible for converting cytosolic acyl CoA and free carnitine to acyl carnitine and free CoA. CoA does not pass through the inner mitochondrial membrane, and CPT1 is used to transfer the acyl group to carnitine *to generate* acyl carnitine*, which can be* transported *by the carnitine/acyl carnitine carrier* across the inner mitochondrial membrane in exchange for mitochondrial free carnitine. CPT2 *on* the inner mitochondrial membrane catalyzes the transfer of the acyl group from carnitine to free CoA *to generate* free carnitine. This series of enzymes serves to transfer acyl CoA to the mitochondria, where it undergoes beta oxidation. *Therefore,* a decrease in *the* level or activity of CPT1 would reduce beta oxidation and reduce the level of long chain acyl carnitines. The mechanism by which loss of CypD leads to the ~23% decrease in CPT1 (Table 2) is unclear and will require further study. However, consistent with the data in our

study, inhibition of CPT1 would lead to an increase in BCAA catabolism to provide additional *sources* of acetyl and succinyl CoA.

In summary, using a proteomics approach, we find that mice lacking CypD have a number of protein changes that are associated several pathways including BCAA degradation, citric acid cycle and pyruvate metabolism. We found that these changes in metabolic pathways were not due to alterations in SDH or the ETFDH. We found a ~23% decrease in CPT1 along with a decrease in acyl carnitine levels in the heart. This inhibition of CPT1 would alter numerous metabolic pathways consistent with our results and would increase BCAA catabolism. The inhibition of CPT1 would also be consistent with previous studies showing that $CypD^{-/-}$ hearts had reduced oxidation of fatty acid and increased oxidation of glucose [6]. The increase in glucose oxidation in the $CypD^{-/-}$ hearts would also be consistent with increased MAS activity, which would be needed to transfer glycolytically generated NADH in the cytosol to the mitochondrial matrix. Taken together, these data show that there are many metabolic changes in the $CypD^{-/-}$ mice and that caution should be used when interpreting results from these mice as due solely to inhibition of the MPTP.

Acknowledgments

We thank the Sanford Burnham Metabolomics core facility *for the metabolomics measurements*. This work was supported by the Intramural Program of the National Heart, Lung, and Blood Institute, NIH.

References

1. Di Lisa F, Carpi A, Giorgio V, Bernardi P. The mitochondrial permeability transition pore and cyclophilin D in cardioprotection. Biochim Biophys Acta. 2011; 1813:1316–1322. [PubMed: 21295622]
2. Tanveer A, Virji S, Andreeva L, Totty NF, Hsuan JJ, Ward JM, et al. Involvement of cyclophilin D in the activation of a mitochondrial pore by Ca2+ and oxidant stress. Eur J Biochem. 1996; 238:166–172. [PubMed: 8665934]
3. Connern CP, Halestrap AP. Purification and N-terminal sequencing of peptidyl-prolyl cis-trans-isomerase from rat liver mitochondrial matrix reveals the existence of a distinct mitochondrial cyclophilin. Biochem J. 1992; 284 (Pt 2):381–385. [PubMed: 1599421]
4. Baines CP, Kaiser RA, Purcell NH, Blair NS, Osinska H, Hambleton MA, et al. Loss of cyclophilin D reveals a critical role for mitochondrial permeability transition in cell death. Nature. 2005; 434:658–662. [PubMed: 15800627]
5. Nakagawa T, Shimizu S, Watanabe T, Yamaguchi O, Otsu K, Yamagata H, et al. Cyclophilin D-dependent mitochondrial permeability transition regulates some necrotic but not apoptotic cell death. Nature. 2005; 434:652–658. [PubMed: 15800626]
6. Elrod JW, Wong R, Mishra S, Vagnozzi RJ, Sakthievel B, Goonasekera SA, et al. Cyclophilin D controls mitochondrial pore-dependent Ca(2+) exchange, metabolic flexibility, and propensity for heart failure in mice. J Clin Invest. 2010; 120:3680–3687. [PubMed: 20890047]
7. Ramachandran A, Lebofsky M, Baines CP, Lemasters JJ, Jaeschke H. Cyclophilin D deficiency protects against acetaminophen-induced oxidant stress and liver injury. Free Radic Res. 2011; 45:156–164. [PubMed: 20942566]
8. Hausenloy DJ, Lim SY, Ong SG, Davidson SM, Yellon DM. Mitochondrial cyclophilin-D as a critical mediator of ischaemic preconditioning. Cardiovasc Res. 88:67–74. [PubMed: 20400621]
9. Devalaraja-Narashimha K, Diener AM, Padanilam BJ. Cyclophilin D deficiency prevents diet-induced obesity in mice. FEBS Lett. 2011; 585:677–682. [PubMed: 21276794]
10. Luvisetto S, Basso E, Petronilli V, Bernardi P, Forte M. Enhancement of anxiety, facilitation of avoidance behavior, and occurrence of adult-onset obesity in mice lacking mitochondrial cyclophilin D. Neuroscience. 2008; 155:585–596. [PubMed: 18621101]

11. Du H, Guo L, Fang F, Chen D, Sosunov AA, McKhann GM, et al. Cyclophilin D deficiency attenuates mitochondrial and neuronal perturbation and ameliorates learning and memory in Alzheimer's disease. Nat Med. 2008; 14:1097–1105. [PubMed: 18806802]
12. Bernardi P, Petronilli V. The permeability transition pore as a mitochondrial calcium release channel: a critical appraisal. J Bioenerg Biomembr. 1996; 28:131–138. [PubMed: 9132411]
13. Halestrap AP. What is the mitochondrial permeability transition pore? J Mol Cell Cardiol. 2009; 46:821–831. [PubMed: 19265700]
14. Piot C, Croisille P, Staat P, Thibault H, Rioufol G, Mewton N, et al. Effect of cyclosporine on reperfusion injury in acute myocardial infarction. N Engl J Med. 2008; 359:473–481. [PubMed: 18669426]
15. Griffiths EJ, Halestrap AP. Protection by Cyclosporin A of ischemia/reperfusion-induced damage in isolated rat hearts. J Mol Cell Cardiol. 1993; 25:1461–1469. [PubMed: 7512654]
16. Halestrap AP, Clarke SJ, Javadov SA. Mitochondrial permeability transition pore opening during myocardial reperfusion--a target for cardioprotection. Cardiovasc Res. 2004; 61:372–385. [PubMed: 14962470]
17. Gomez L, Thibault H, Gharib A, Dumont JM, Vuagniaux G, Scalfaro P, et al. Inhibition of mitochondrial permeability transition improves functional recovery and reduces mortality following acute myocardial infarction in mice. Am J Physiol Heart Circ Physiol. 2007; 293:H1654–1661. [PubMed: 17557911]
18. Hausenloy DJ, Duchen MR, Yellon DM. Inhibiting mitochondrial permeability transition pore opening at reperfusion protects against ischaemia-reperfusion injury. Cardiovasc Res. 2003; 60:617–625. [PubMed: 14659807]
19. Scholz TD, Balaban RS. Mitochondrial F1-ATPase activity of canine myocardium: effects of hypoxia and stimulation. Am J Physiol. 1994; 266:H2396–2403. [PubMed: 8024001]
20. Hopper RK, Carroll S, Aponte AM, Johnson DT, French S, Shen RF, et al. Mitochondrial matrix phosphoproteome: effect of extra mitochondrial calcium. Biochemistry. 2006; 45:2524–2536. [PubMed: 16489745]
21. Boja ES, Phillips D, French SA, Harris RA, Balaban RS. Quantitative mitochondrial phosphoproteomics using iTRAQ on an LTQ-Orbitrap with high energy collision dissociation. J Proteome Res. 2009; 8:4665–4675. [PubMed: 19694452]
22. Amendt BA, Rhead WJ. The multiple acyl-coenzyme A dehydrogenation disorders, glutaric aciduria type II and ethylmalonic-adipic aciduria. Mitochondrial fatty acid oxidation, acyl-coenzyme A dehydrogenase, and electron transfer flavoprotein activities in fibroblasts. J Clin Invest. 1986; 78:205–213. [PubMed: 3722376]
23. Birch-Machin MA, Turnbull DM. Assaying mitochondrial respiratory complex activity in mitochondria isolated from human cells and tissues. Methods Cell Biol. 2001; 65:97–117. [PubMed: 11381612]
24. Contreras L, Satrustegui J. Calcium signaling in brain mitochondria: interplay of malate aspartate NADH shuttle and calcium uniporter/mitochondrial dehydrogenase pathways. J Biol Chem. 2009; 284:7091–7099. [PubMed: 19129175]
25. Petucci C, Rojas-Betancourt S, Gardell SJ. Comparison of tissue harvest protocols for the quantitation of acylcarnitines in mouse heart and liver by mass spectrometry. Metabolomics. 2012 in press.
26. Ghosh JC, Siegelin MD, Dohi T, Altieri DC. Heat shock protein 60 regulation of the mitochondrial permeability transition pore in tumor cells. Cancer Res. 2010; 70:8988–8993. [PubMed: 20978188]
27. Woodfield K, Ruck A, Brdiczka D, Halestrap AP. Direct demonstration of a specific interaction between cyclophilin-D and the adenine nucleotide translocase confirms their role in the mitochondrial permeability transition. Biochem J. 1998; 336 (Pt 2):287–290. [PubMed: 9820802]
28. Leung AW, Varanyuwatana P, Halestrap AP. The mitochondrial phosphate carrier interacts with cyclophilin D and may play a key role in the permeability transition. J Biol Chem. 2008; 283:26312–26323. [PubMed: 18667415]

29. Giorgio V, Bisetto E, Soriano ME, Dabbeni-Sala F, Basso E, Petronilli V, et al. Cyclophilin D modulates mitochondrial F0F1-ATP synthase by interacting with the lateral stalk of the complex. J Biol Chem. 2009; 284:33982–33988. [PubMed: 19801635]

30. Kang BH, Plescia J, Dohi T, Rosa J, Doxsey SJ, Altieri DC. Regulation of tumor cell mitochondrial homeostasis by an organelle-specific Hsp90 chaperone network. Cell. 2007; 131:257–270. [PubMed: 17956728]

31. Eliseev RA, Malecki J, Lester T, Zhang Y, Humphrey J, Gunter TE. Cyclophilin D interacts with Bcl2 and exerts an anti-apoptotic effect. J Biol Chem. 2009; 284:9692–9699. [PubMed: 19228691]

32. Vaseva AV, Marchenko ND, Ji K, Tsirka SE, Holzmann S, Moll UM. p53 opens the mitochondrial permeability transition pore to trigger necrosis. Cell. 2012; 149:1536–1548. [PubMed: 22726440]

Highlights

- Identification of proteomic differences between WT and CypD$^{-/-}$ mice.
- CypD$^{-/-}$ mice have many protein changes associated to several metabolic pathways.
- These changes in metabolic pathways are not due to alterations in electron transfer.
- CypD$^{-/-}$ hearts have reduced oxidation of fatty acid and increased oxidation of glucose.
- Results from CypD$^{-/-}$ mice may not be solely due to MPTP inhibition.

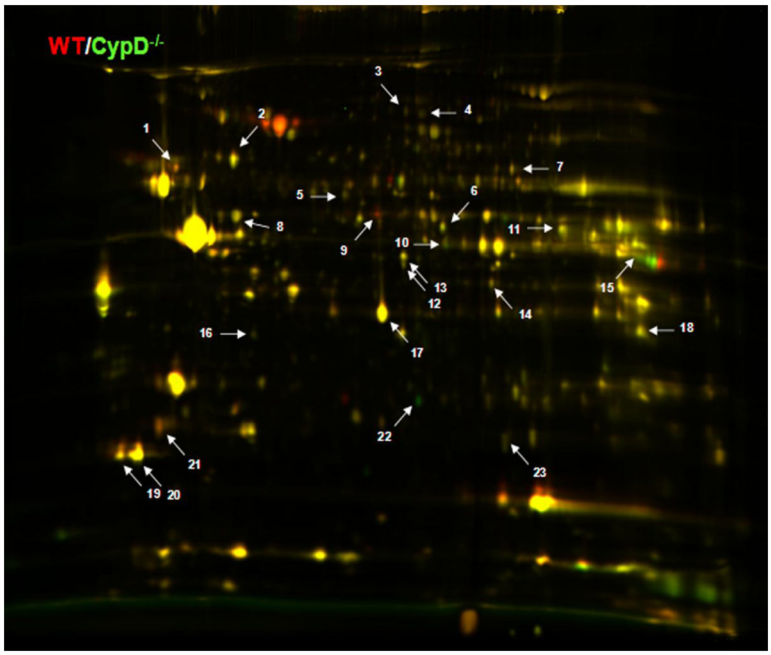

Figure 1.

Proteome of total heart homogenate from WT and CypD$^{-/-}$ *male and femal* mice. Representative two-dimensional difference gel electrophoresis (2D-DIGE) image of proteins from WT (labeled green, Cy3) and CypD$^{-/-}$ *female* (labeled red, Cy5) heart homogenates. All experiments were performed in triplicates *using adult male and female mice,* and arrows indicate protein spots of interest. *Similar differences between CypD−/− and WT were found in males and females.*

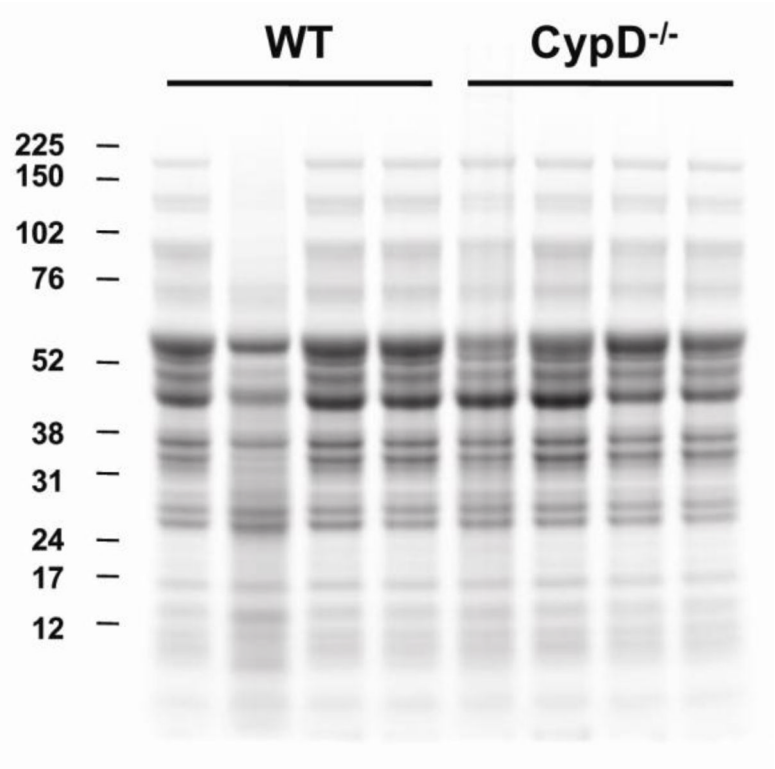

Figure 2.
Mitochondrial fraction preparation for iTRAQ labeling. Representative Coomassie-stained SDS-PAGE gels of mitochondrial fractions isolated from WT *(2 M and 2 F)* and $CypD^{-/-}$ *(2M and 2F)* hearts. *Similar differences between CypD−/− and WT were found in males and females.*

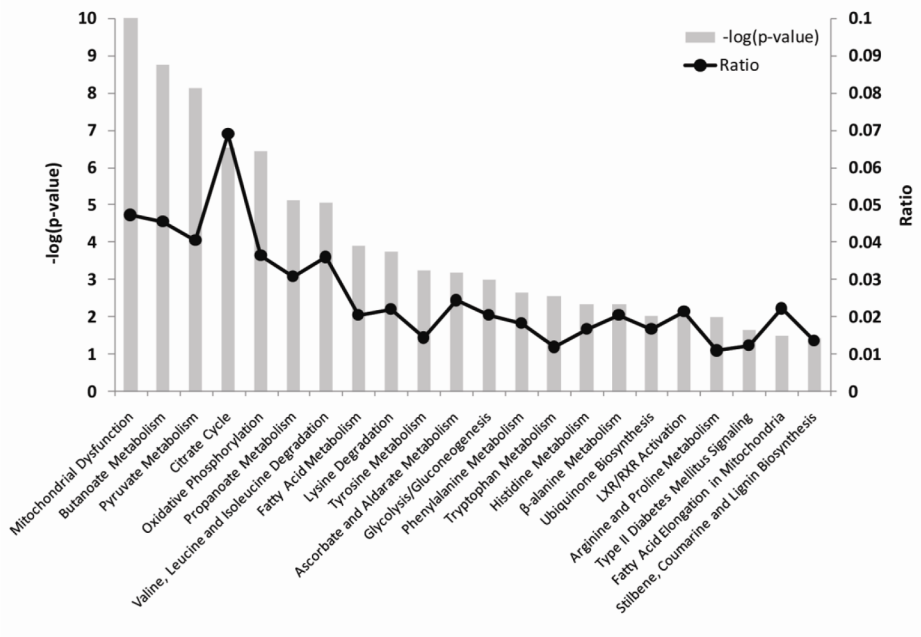

Fig. 3A

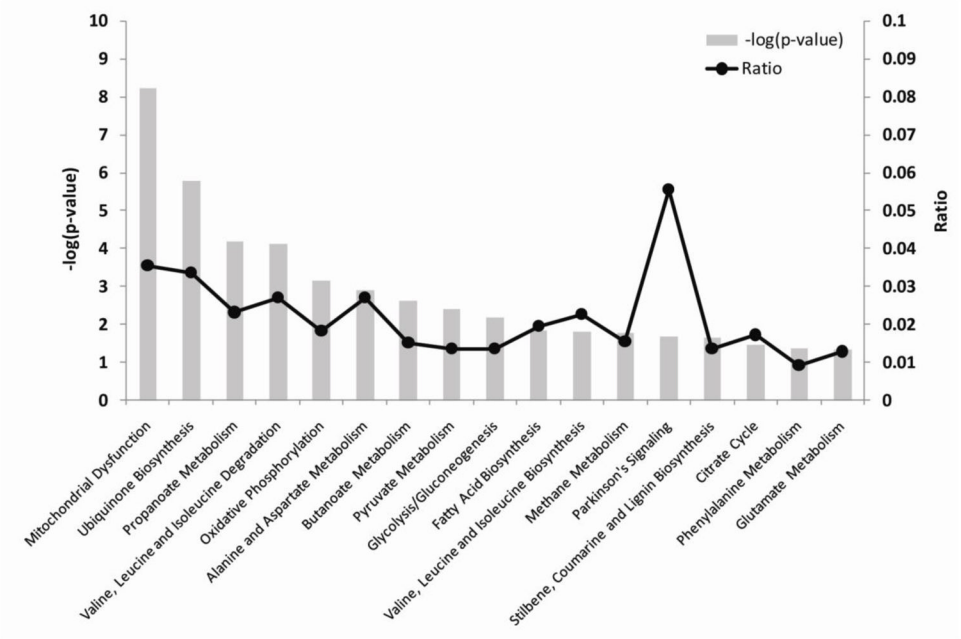

Fig. 3B

Figure 3.

The top canonical pathways associated with the CypD$^{-/-}$ iTRAQ decreases and increases. *Isolated mitochondria from two male and two female CypD$^{-/-}$ and WT mouse hearts were used for iTRAQ analysis.* Ingenuity Pathway Analysis was performed on iTRAQ proteins that were increased and decreased in CypD$^{-/-}$ compared to WT. *The left* axis is the −log (*p*-value), where the *p*-value (Fisher's test) is the probability that the association of the proteins in the dataset and the canonical pathway is explained by chance alone. *The right* axis is the

ratio of the number of proteins that map to a specific pathway divided by the total number of proteins in Table 2 or 3.

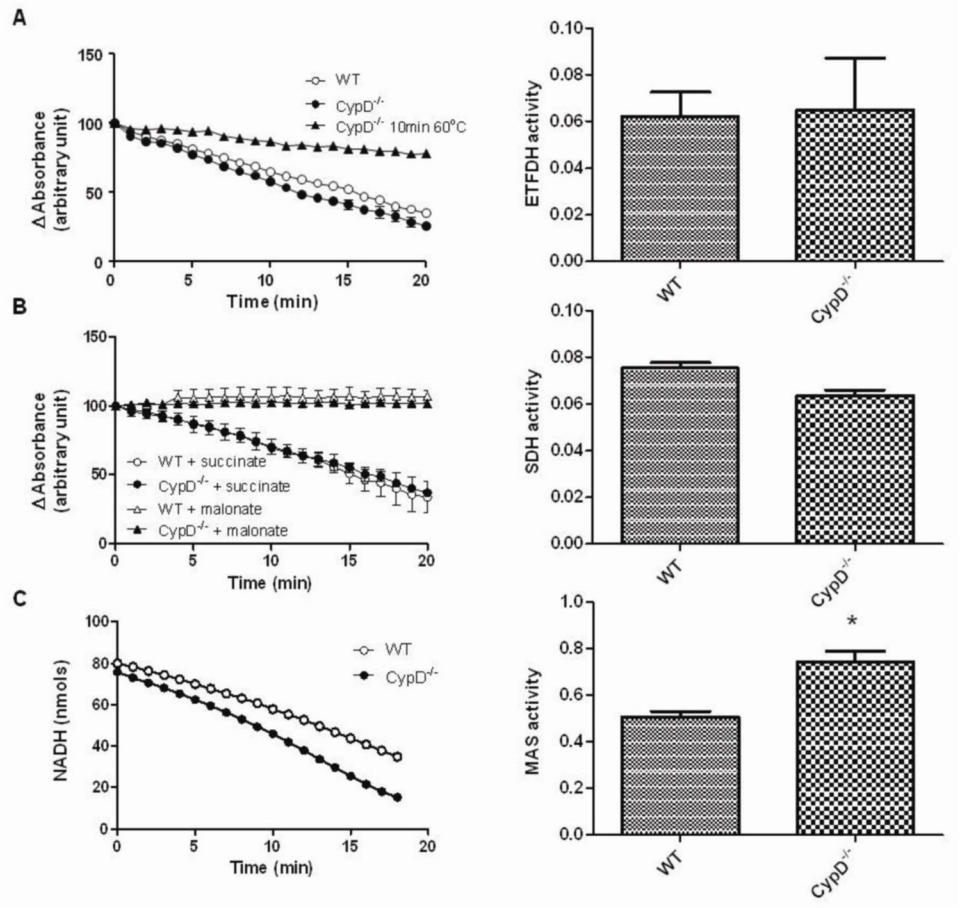

Figure 4.

Metabolic changes in CypD$^{-/-}$ hearts. (A) ETFDH activity in WT and CypD$^{-/-}$ hearts showed no difference between groups. ETFDH activity was measured by *the* change in absorbance of DCIP (left panel). The right panel shows the mean and SE for the rate of reduction o*f* the DCIP, *which was* calculated from the change in absorbance during the first 10 minutes. (B) Mitochondria from WT and CypD$^{-/-}$ hearts showed no change in SDH activity. In *the* left panel, SDH activity was measured by following the reduction of DCIP. The graph in the right panel shows *the* mean and SE for the rate of reduction of DCIP, *which was* calculated during the first 10 minutes of the reaction. (C) Malate-aspartate shuttle capacity is increased in CypD$^{-/-}$ compared to WT mitochondria. Shuttle activity was followed by measuring *NADH* oxidation as a function of time (left panel). The graph in the right panel shows *the* mean and SE for the rate of reduction of NADH fluorescence, *which was* calculated from the change in fluorescence during the first 10 minutes of the reaction. All experiments were performed in triplicates *using adult male mice.* Data are means ± S.E. *, p≤0.05.

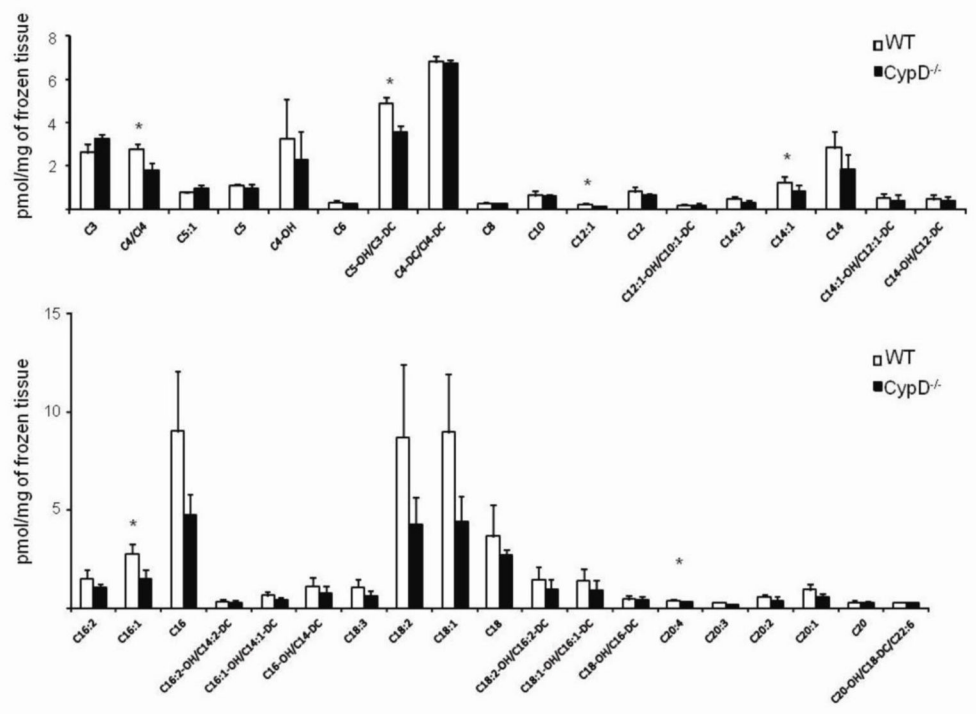

Figure 5.

Metabolomic analysis of acyl carnitines showed a significant decrease in C4/Ci4, C5-OH/C3-DC, C12:1, C14:1, C16:1, and C20:3 in hearts from CypD$^{-/-}$ mice. *Adult male mice were used in this experiment.* Data (n=3 *in each group*) are mean ± S.D. *, p≤0.05.

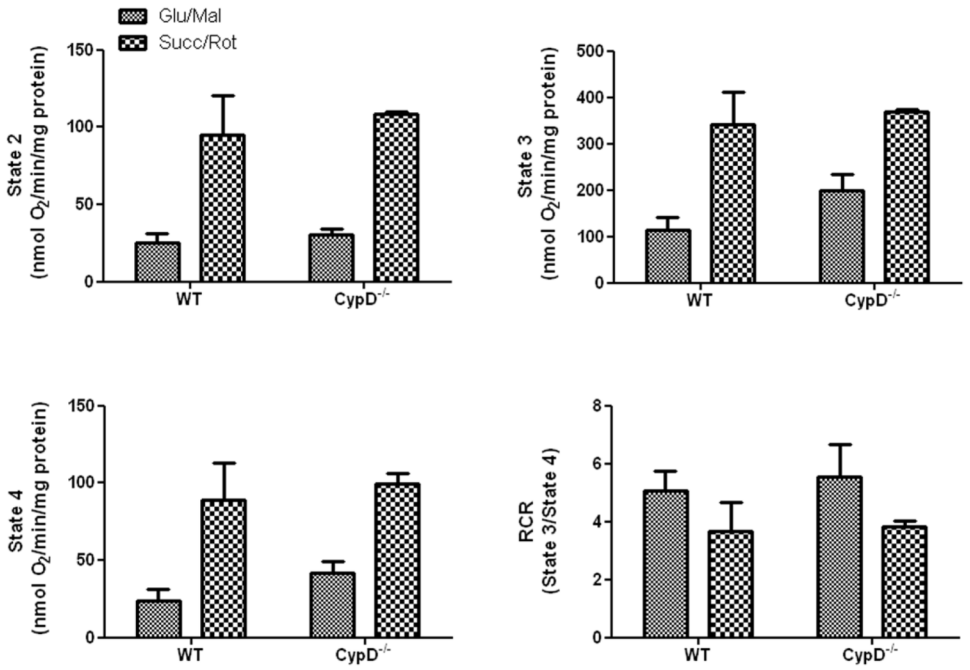

Figure 6.

Oxygen consumption in WT and CypD$^{-/-}$ mitochondria (n = 3 in each group) with 10 mM glutamate/2 mM malate and 5 mM succinate/2 μM rotenone. *Adult male mice were used in this experiment.*

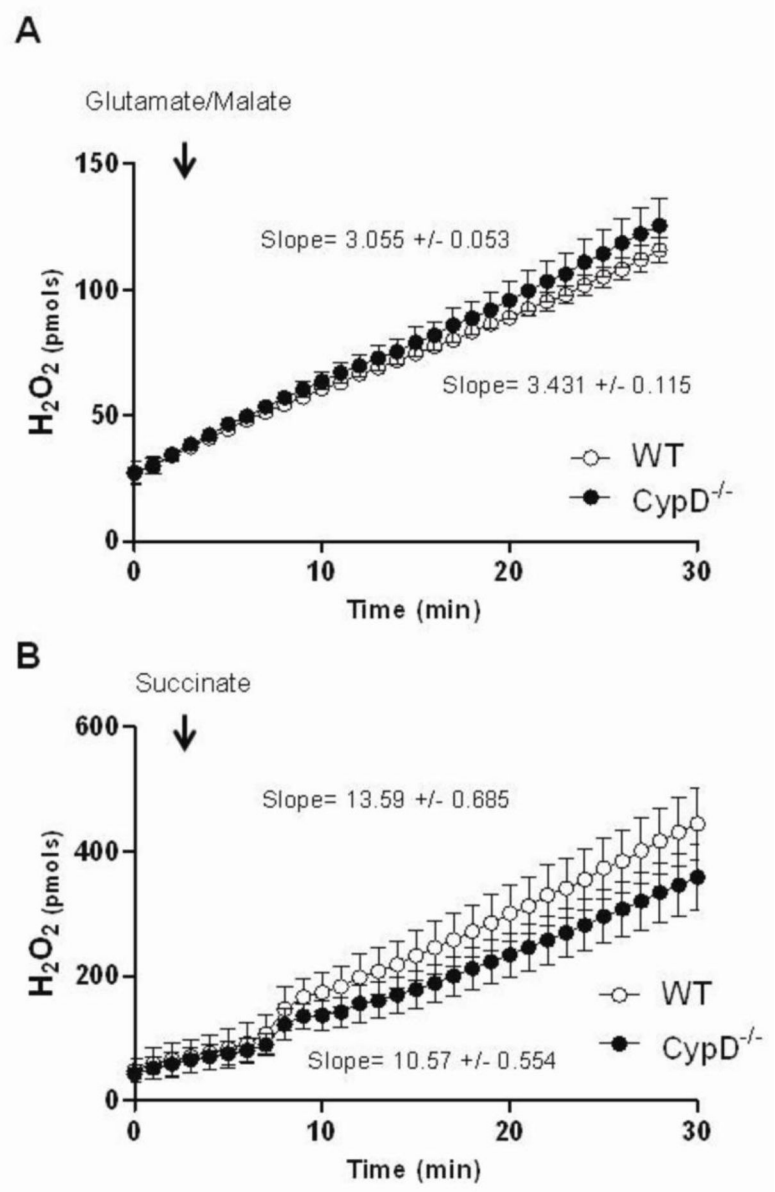

Figure 7.

H_2O_2 production measured by Amplex Red under normoxic conditions is unchanged between WT and $CypD^{-/-}$ mitochondria (n = 3 in each group) both given 10 mM glutamate/ 2 mM malate or 10 mM succinate as substrates. *Adult male mice were used in this experiment.*

Table 1

WT/CypD$^{-/-}$ Heart 2D DIGE Protein Differences

Spot #	Protein Name	Accession Number	Protein MW	Peptide Count	Total Ion Score	Effect in CypD$^{-/-}$ (KO)		*p*
1	(P20152) Vimentin.	VIME_MOUSE	53712	4	98.42%	28%	lower in KO	0.022
2	(P63038) 60 kDa heat shock protein, mitochondrial precursor	CH60_MOUSE	61088	4	99.09%	11%	higher in KO	0.027
3	(Q91ZA3) Propionyl-CoA carboxylase alpha chain, mitochondrial precursor	PCCA_MOUSE	78289	5	99.63%	7%	lower in KO	0.018
4	(Q99NB1) Acetyl-coenzyme A synthetase 2-like, mitochondrial precursor	ACS2L_MOUSE	75317	4	100.00%	14%	lower in KO	0.025
5	(Q9D2G2) Dihydrolipoyllysine-residue succinyltransferase component of 2-oxoglutarate dehydrogenase	ODO2_MOUSE	49236	6	100.00%	10%	higher in KO	0.050
6	(Q8BFR5) Elongation factor Tu, mitochondrial precursor	EFTU_MOUSE	49876	6	100.00%	18%	higher in KO	0.028
7	(P52480) Pyruvate kinase isozymes M1/M2	KPYM_MOUSE	58294	3	99.94%	9%	lower in KO	0.049
8	(Q9CZ13) Cytochrome b-c1 complex subunit 1, mitochondrial precursor	QCR1_MOUSE	53420	6	100.00%	7%	higher in KO	0.054
9	(P35486) Pyruvate dehydrogenase E1 component subunit alpha, somatic form	ODPA_MOUSE	43888	3	99.98%	28%	lower in KO	0.037
10	(P51174) Long-chain specific acyl-CoA dehydrogenase, mitochondrial precursor	ACADL_MOUSE	48242	2	99.98%	27%	higher in KO	0.016
11	(Q6P8J7) Creatine kinase, sarcomeric mitochondrial precursor	KCRS_MOUSE	47811	4	100.00%	31%	higher in KO	0.021
12	(Q99LC3) NADH dehydrogenase [ubiquinone] 1 alpha subcomplex subunit 10	NDUAA_MOUSE	40863	2	98.90%	10%	higher in KO	0.054
13	(Q99LC3) NADH dehydrogenase [ubiquinone] 1 alpha subcomplex subunit 10	NDUAA_MOUSE	40863	4	99.89%	7%	higher in KO	0.049
14	(P45376) Aldose reductase	ALDR_MOUSE	36052	4	100.00%	9%	lower in KO	0.001
15	(P05064) Fructose-bisphosphate aldolase A	ALDOA_MOUSE	39783	4	100.00%	39%	higher in KO	0.048
16	(P67778) Prohibitin	PHB_MOUSE	29859	4	100.00%	17%	higher in KO	0.015
17	(P14152) Malate dehydrogenase, cytoplasmic	MDHC_MOUSE	36659	8	100.00%	13%	lower in KO	0.054
18	(Q91VR2) ATP synthase subunit gamma, mitochondrial	ATPG_MOUSE	30229	4	100.00%	7%	higher in KO	0.054
19	(P51667) Myosin regulatory light chain 2, ventricular/cardiac muscle isoform	MLRV_MOUSE	18868	3	99.97%	30%	lower in KO	0.029
20	(P51667) Myosin regulatory light chain 2, ventricular/cardiac muscle isoform	MLRV_MOUSE	18868	6	100.00%	18%	lower in KO	0.020
21	(P09541) Myosin light chain 4	MYL4_MOUSE	21383	5	100.00%	29%	lower in KO	0.040
22	(O08709) Peroxiredoxin-6	PRDX6_MOUSE	24969	4	99.99%	283%	higher in KO	< 0.001
23	(P23927) Alpha-crystallin B chain	CRYAB_MOUSE	20056	2	99.87%	20%	higher in KO	0.054

Spots were picked based on $p \leq 0.05$ from three biological replicates. Identifications were confirmed by MS/MS in at least two separate gels and with at least 2 unique peptides. Data are expressed as percent change in $CypD^{-/-}$ (KO) compared to WT. Accession numbers are from the SWISSPROT/Uniprot database.

Table 2

CypD$^{-/-}$ Heart Mitochondrial Protein Decreases Relative to WT

Protein Name	Accession Number	Coverage	# Peptides	iTRAQ Ratio		*p*	% change
				WT/WT	KO/WT		
(P15864) Histone H1.2	H12_MOUSE	7.08	2	0.823 ± 0.077	0.157 ± 0.027	<0.001	−80
(Q3TLP5) Enoyl-CoA hydratase domain-containing protein 2, mitochondrial	ECHD2_MOUSE	12.84	5	0.858 ± 0.053	0.565 ± 0.019	0.002	−34
(Q8CIM3) D-2-hydroxyglutarate dehydrogenase, mitochondrial	D2HDH_MOUSE	12.15	6	0.964 ± 0.038	0.674 ± 0.057	0.005	−30
(Q8BH86) UPF0317 protein C14orf159 homolog, mitochondrial	CN159_MOUSE	3.57	3	0.975 ± 0.069	0.702 ± 0.064	0.027	−28
(Q9CZB0) Succinate dehydrogenase cytochrome b560 subunit, mitochondrial	C560_MOUSE	28.99	22	1.015 ± 0.061	0.764 ± 0.034	0.011	−25
(Q924X2) Carnitine O-palmitoyltransferase 1, muscle isoform	CPT1B_MOUSE	32.77	52	0.975 ± 0.038	0.748 ± 0.018	0.002	−23
(O88441) Metaxin-2	MTX2_MOUSE	45.63	8	0.946 ± 0.032	0.745 ± 0.068	0.036	−21
(Q05920) Pyruvate carboxylase, mitochondrial	PYC_MOUSE	3.74	4	0.943 ± 0.037	0.742 ± 0.033	0.006	−21
(Q08857) Platelet glycoprotein 4	CD36_MOUSE	15.25	7	0.938 ± 0.059	0.753 ± 0.038	0.038	−20
(Q61941) NAD(P) transhydrogenase, mitochondrial	NNTM_MOUSE	35.08	197	1.067 ± 0.044	0.858 ± 0.029	0.007	−20
(P56391) Cytochrome c oxidase subunit 6B1	CX6B1_MOUSE	48.84	14	1.022 ± 0.023	0.822 ± 0.040	0.005	−20
(Q791V5) Mitochondrial carrier homolog 2	MTCH2_MOUSE	33.00	22	0.984 ± 0.006	0.797 ± 0.033	0.001	−19
(P53395) Lipoamide acyltransferase component of branched-chain alpha-keto acid dehydrogenase complex, mitochondrial	ODB2_MOUSE	6.43	3	0.877 ± 0.053	0.718 ± 0.018	0.031	−18
(Q9CQA3) Succinate dehydrogenase [ubiquinone] iron-sulfur subunit, mitochondrial	DHSB_MOUSE	51.06	77	1.079 ± 0.048	0.899 ± 0.051	0.042	−17
(Q99NB1) Acetyl-coenzyme A synthetase 2-like, mitochondrial	ACS2L_MOUSE	22.87	24	0.969 ± 0.023	0.819 ± 0.035	0.012	−15
(Q9CR62) Mitochondrial 2-oxoglutarate/malate carrier protein	M2OM_MOUSE	53.50	299	0.990 ± 0.024	0.837 ± 0.026	0.005	−15
(Q9DB73) NADH-cytochrome b5 reductase 1	NB5R1_MOUSE	11.80	3	0.897 ± 0.045	0.766 ± 0.031	0.053	−15
(P47738) Aldehyde dehydrogenase, mitochondrial	ALDH2_MOUSE	22.54	23	0.945 ± 0.041	0.812 ± 0.033	0.044	−14
(Q8K2B3) Succinate dehydrogenase [ubiquinone] flavoprotein subunit, mitochondrial	DHSA_MOUSE	55.42	323	0.957 ± 0.044	0.823 ± 0.030	0.046	−14
(Q6P3A8) 2-oxoisovalerate dehydrogenase subunit beta, mitochondrial	ODBB_MOUSE	12.05	5	0.981 ± 0.023	0.844 ± 0.034	0.017	−14
(P41216) Long-chain-fatty-acid--CoA ligase 1	ACSL1_MOUSE	38.63	83	0.918 ± 0.034	0.793 ± 0.011	0.013	−14
(Q8BMF3) NADP-dependent malic enzyme, mitochondrial	MAON_MOUSE	14.74	5	1.070 ± 0.024	0.931 ± 0.051	0.049	−13
(Q8VEM8) Phosphate carrier protein, mitochondrial	MPCP_MOUSE	44.82	210	1.001 ± 0.031	0.877 ± 0.023	0.018	−12
(Q60931) Voltage-dependent anion-selective channel protein 3	VDAC3_MOUSE	33.92	45	0.976 ± 0.014	0.860 ± 0.038	0.029	−12
(P20108) Thioredoxin-dependent peroxide reductase, mitochondrial	PRDX3_MOUSE	30.74	44	0.948 ± 0.023	0.840 ± 0.008	0.005	−11
(Q99LC5) Electron transfer flavoprotein subunit alpha, mitochondrial	ETFA_MOUSE	66.97	265	1.044 ± 0.020	0.953 ± 0.017	0.014	−9
(Q9DCW4) Electron transfer flavoprotein subunit beta	ETFB_MOUSE	61.96	85	0.987 ± 0.015	0.905 ± 0.018	0.013	−8

Protein Name	Accession Number	Coverage	# Peptides	iTRAQ Ratio		*p*	% change
				WT/WT	KO/WT		
(Q91YT0) NADH dehydrogenase [ubiquinone] flavoprotein 1, mitochondrial	NDUV1_MOUSE	40.52	42	1.070 ± 0.032	0.984 ± 0.014	0.050	−8
(Q8BH95) Enoyl-CoA hydratase, mitochondrial	ECHM_MOUSE	38.28	52	1.035 ± 0.012	0.956 ± 0.017	0.009	−8
(Q9DB77) Cytochrome b-c1 complex subunit 2, mitochondrial	QCR2_MOUSE	53.42	131	0.986 ± 0.012	0.912 ± 0.024	0.032	−8

Fold changes in protein levels were expressed as the iTRAQ reporter ion ratios of WT or CypD$^{-/-}$ (KO) in reference to WT (Mean ± SE). Proteins were identified based on a false discovery rate of $p<0.01$ from four replicates and $p \leq 0.05$. Identifications were confirmed by MS/MS and with at least 2 unique peptides. Data are expressed as ratios relative to WT. Accession numbers are from the SWISSPROT/Uniprot database.

J Mol Cell Cardiol. Author manuscript; available in PMC 2014 March 01.

Table 3

CypD$^{-/-}$ Heart Mitochondrial Protein Increases Relative to WT

Protein Name	Accession Number	Coverage	# Peptides	iTRAQ Ratios		*p*	% change
				WT/WT	KO/WT		
(O09111) NADH dehydrogenase [ubiquinone] 1 beta subcomplex subunit 11, mitochondrial	NDUBB_MOUSE	17.88	3	1.280 ± 0.130	5.640 ± 0.304	<0.001	340
(Q99MR8) Methylcrotonoyl-CoA carboxylase subunit alpha, mitochondrial	MCCA_MOUSE	7.11	5	1.080 ± 0.080	1.915 ± 0.091	<0.001	77
(Q99J99) 3-mercaptopyruvate sulfurtransferase	THTM_MOUSE	7.74	2	1.242 ± 0.108	1.967 ± 0.129	0.005	58
(P56379) 6.8 kDa mitochondrial proteolipid	68MP_MOUSE	29.31	11	0.926 ± 0.036	1.330 ± 0.099	0.009	44
(Q3ULD5) Methylcrotonoyl-CoA carboxylase beta chain, mitochondrial	MCCB_MOUSE	18.83	11	1.139 ± 0.071	1.615 ± 0.018	0.001	42
(Q8CC88) Uncharacterized protein KIAA0564 homolog	K0564_MOUSE	2.73	6	0.858 ± 0.053	1.098 ± 0.031	0.008	28
(Q9R112) Sulfide:quinone oxidoreductase, mitochondrial	SQRD_MOUSE	13.33	6	1.056 ± 0.061	1.328 ± 0.070	0.027	26
(Q8BMS4) Hexaprenyldihydroxybenzoate methyltransferase, mitochondrial	COQ3_MOUSE	15.41	7	0.988 ± 0.019	1.187 ± 0.027	0.001	20
(P42125) 3,2-trans-enoyl-CoA isomerase, mitochondrial	D3D2_MOUSE	42.56	69	0.979 ± 0.030	1.166 ± 0.033	0.006	19
(Q9D1I6) 39S ribosomal protein L14, mitochondrial	RM14_MOUSE	13.10	2	0.902 ± 0.036	1.071 ± 0.022	0.007	19
(Q9Z2I8) Succinyl-CoA ligase [GDP-forming] subunit beta, mitochondrial	SUCB2_MOUSE	23.56	9	0.985 ± 0.027	1.149 ± 0.021	0.003	17
(Q99LX0) Protein DJ-1	PARK7_MOUSE	21.69	4	0.990 ± 0.007	1.138 ± 0.021	<0.001	15
(P99029) Peroxiredoxin-5, mitochondrial	PRDX5_MOUSE	50.48	38	0.990 ± 0.030	1.136 ± 0.045	0.035	15
(Q9DCJ5) NADH dehydrogenase [ubiquinone] 1 alpha subcomplex subunit 8	NDUA8_MOUSE	50.00	18	0.987 ± 0.015	1.129 ± 0.049	0.032	14
(P63038) 60 kDa heat shock protein, mitochondrial	CH60_MOUSE	54.10	326	0.997 ± 0.025	1.139 ± 0.053	0.052	14
(P16332) Methylmalonyl-CoA mutase, mitochondrial	MUTA_MOUSE	10.56	6	0.932 ± 0.027	1.055 ± 0.026	0.017	13
(P35486) Pyruvate dehydrogenase E1 component subunit alpha, somatic form, mitochondrial	ODPA_MOUSE	50.77	55	1.060 ± 0.029	1.178 ± 0.013	0.009	11
(Q8BMF4) Dihydrolipoyllysine-residue acetyltransferase component of pyruvate dehydrogenase complex, mitochondrial	ODP2_MOUSE	26.32	56	1.013 ± 0.019	1.126 ± 0.026	0.014	11
(Q99J39) Malonyl-CoA decarboxylase, mitochondrial	DCMC_MOUSE	11.38	7	1.036 ± 0.013	1.149 ± 0.041	0.039	11
(Q9CPP6) NADH dehydrogenase [ubiquinone] 1 alpha subcomplex subunit 5	NDUA5_MOUSE	50.86	20	0.964 ± 0.026	1.055 ± 0.026	0.046	9

Fold changes in protein levels were expressed as the iTRAQ reporter ion ratios of WT or CypD$^{-/-}$ (KO) in reference to WT (Mean ± SE). Proteins were identified based on a false discovery rate of $p<0.01$ from four replicates and $p \leq 0.05$. Identifications were confirmed by MS/MS and with at least 2 unique peptides. Data are expressed as ratios relative to WT. Accession numbers are from the SWISSPROT/Uniprot database.